105 GHz Multipath Propagation Measurements and Path Loss Model for Sub-THz Indoor Short-Range Communications

Yusuke Koda, Norichika Ohmi, Hiroaki Endo, and Hiroshi Harada
Graduate School of Informatics, Kyoto University, Yoshida-honmachi, Sakyo-ku, Kyoto, 606-8501 Japan
{koda@, ohmi@dco.cce., endo@dco.cce., hiroshi.harada@}@i.kyoto-u.ac.jp

***Abstract*—This paper reports a first wideband indoor channel measurement at the 105 GHz sub-terahertz (sub-THz) band and analyzes the multipath characteristics in terms of the omnidirectional path-loss and angular characteristics. The measurement campaigns with the 4 GHz bandwidth are performed focusing on indoor short-range communication scenarios in a conference room, corridor, and office room, which have been considered in the primary 60 GHz communication systems standardized by the IEEE 802.15.3c/11ad. Moreover, to draw full understanding to scale the 60 GHz indoor channel models and 60 GHz system designs for the 105 GHz band, we also conduct 60 GHz channel measurements in the same environment with few modifications in the channel-sounding system and performed the comparison between these two bands. Based on these measurements, we demonstrate the affinity that exists between 105 GHz and 60 GHz bands in terms of path loss exponent and angular characteristics of multipath components, shedding light on the hypothesis that several system designs of the 60 GHz communication systems (e.g., beam switching for non-line-of sight conditions) can be applied to the 105 GHz sub-THz communication systems.**

Keywords—sub-terahertz, propagation measurement, path-loss model, multi-path characteristics, short-range communication

I. Introduction

As the fifth-generation (5G) mobile communication systems become widespread, the next-generation communication systems will witness a huge demand to realize a higher peak rate, more massive connectivity, and ultra-reliability [1]. To combat the spectrum scarcity incurred by such demands, the frequency spectrum above 100 GHz–300 GHz and beyond has attracted increasing attention. Particularly, the former frequency band ranging from 100 GHz to 300 GHz is often referred to as the sub-terahertz (sub-THz) band, which is one of the central topics to support the next-generation wireless communication systems.

Recently, to draw an understanding of these sub-THz band, the channel measurements have been performed in several institutions worldwide. For example, indoor channel measurements at the 300 GHz band have been extensively conducted [2–5]. This is due to the fact that this band was chosen as the operating band of the first THz communication system standardized by the IEEE 802.15.3d task group [6], where the channel characterization at this band should naturally be the topic of interest. As for the other sub-THz band, New York University performed extensive channel measurements at the 140 GHz with a bandwidth of 1 GHz for office [7], industry [8], and outdoor urban microcell (UMi) scenarios [9] and developed the complete channel generation framework as a simulator called NYUSIM. Laboratoire d'électronique des technologies de l'information performed an indoor measurement at 126–156 GHz, where the path loss, angular/delay spreads, and human shadowing effects were extensively studied in a laboratory room, conference room, and personal desktop [10]. Aalto University performed the channel measurement at the 140 GHz band in a shopping mall and analyzed the path loss, angular and delay spreads [11]. Moreover, the measurements at the sub-THz bands conducted by other institutions are listed in [12–14].

However, almost all of the works listed above performed the measurements at the bands above 110 GHz, while there are few studies focusing on the multipath characteristics at the band ranging in the 100–110 GHz band. To the best of our knowledge, the only measurement at 100 GHz with the bandwidth of 600 MHz has recently been reported in [15]. This frequency band can be interpreted as the boundary between the millimeter wave (mmWave) and the sub-THz bands, and investigation of this band is also important to fully understand the channel characteristics of the sub-THz band, particularly in comparison to the mmWave band. In more detail, by investigating these bands, we can gain knowledge about how and to what extent the channel models developed for the mmWave bands (e.g., 28 GHz and 60 GHz bands) can be useful for the sub-THz band. This is beneficial because based on this knowledge, we can develop sub-THz channel models by extending the mmWave channel model in a step-by-step manner without developing a new channel model from scratch. Moreover, even if the difference in the channel characteristics between the 100–110 GHz and mmWave bands is insignificant, such insights provide a natural guideline to extend the mmWave communication systems that have been developed so far (e.g., 5G new radio [16], IEEE 802.15.3c 60 GHz wireless personal area network (WPAN) [17], and IEEE 802.11ad wireless local area network (WLAN) [18]) to design the sub-THz band communication systems. To the best of our knowledge, there are no works that discuss this band in comparison with the mmWave channel characteristics.

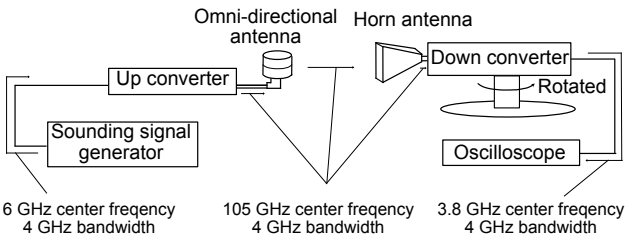

(a) 105 GHz band measurement system.

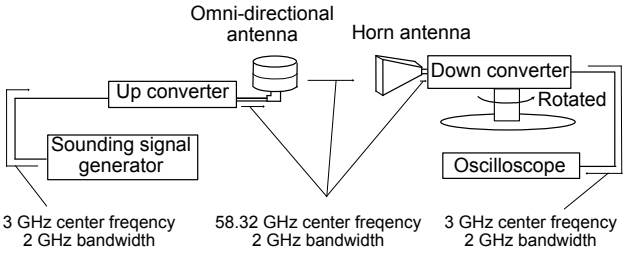

(b) 60 GHz band measurement system.

Fig. 1. Channel-sounding system for 105 GHz and 60 GHz measurements. Note that both receiver horn antennas have identical antenna patterns as illustrated in Fig. 4 later.

Such knowledge should be acquired by comparing the channel characteristics at the 100–110 GHz with those at mmWave bands that are measured at the same locations with few modifications in the channel-sounding systems. Given this background, this paper performs the channel measurement at both 105 GHz and 60 GHz bands in the same environment and compares these two channel characteristics. In more detail, we perform wideband channel measurements of indoor multipath characteristics in the above two bands in an identical measurement environment, such as a conference room desktop, corridor, and office room, which have been considered in the standardization of the 60 GHz WPAN [17] and WLAN systems [18]. Subsequently, we develop a path loss model and analyze the angular characteristics of multipath components, therein. Based on this measurement campaign and analysis, we demonstrate the affinity in the channel characteristics that lie between the 105 GHz and 60 GHz bands. These measurements provide insight that several designs of the 60 GHz WPANs/ WLANs channel models and system components can be applied to the 105 GHz sub-THz band.

II. Measurement Campaigns in 105 GHz Band for Indoor Short-Range Communicaiton

A. Setup of Channel-sounding System

105 GHz channel-sounding system. We developed a channel-sounding system that measures power delay profiles (PDPs) of an omnidirectionally transmitted signal, which is scanned by a rotated receiver (RX) antenna. Fig. 1(a) shows an overview of the channel-sounding system. The RX was equipped with a 25 dBi horn antenna rotatable in the azimuth plane whereas the transmitter (TX) was equipped with an omnidirectional antenna in the azimuth plane. This simple setup was considered backward from the short-range communication use case, where, unlike long-range communication use cases, strict beamforming in both RX and TX sides may not be required. Hence, in contrast to the double-directional measurements generally applied [4], we limited the angular scan only to the RX side while using the omnidirectional antenna on the TX side. As a sounding technique to obtain the PDPs, we applied a Keysight channel-sounding system [19], which is one of the time correlation-based channel-sounding methods. As shown in Fig. 1(a), the signal generator generates the sounding signal with a center frequency of 6 GHz and a bandwidth of 4 GHz. This signal consists of the pseudo-random sequence, which is correlated to the same sequence known also at the RX side with a time resolution of 0.16 ns. Afterward, the sounding signal is up-converted to the radio frequency of 105 GHz and is received in the RX. The received signal is down-converted to the center frequency of 3.8 GHz and is sampled in an oscilloscope. At the same time, the oscilloscope calculates the PDPs based on the time-correlation-based sounding technique. The detailed parameters of this measurement are further shown in Table I.

TABLE I. Parameters in 105 GHz Band Measurement

RF Frequency	105.8 GHz
Center frequency of sounding signal before TX up-conversion	6 GHz
Center frequency of sounding signal before RX down-conversion	3.8 GHz
Channel Bandwidth	4 GHz
Transmit power	5.4 dBm
Receiver sensitivity	-112 dBm (Noise floor -130 dBm + 18 dB margin [21])
Transmitter antenna gain	Omni-directional in azimuth 4 dBi in elevation
Receiver antenna gain	25 dBi
Half power beamwidth of receiver horn antenna	10°
Sampling frequency	16 GHz

TABLE II. Parameters in 60 GHz Band Measurement

RF Frequency	58.32 GHz
Center frequency of sounding signal	3 GHz
Channel Bandwidth	2 GHz
Transmit power	8.6 dBm
Receiver sensitivity	-127 dBm (Noise floor -145 dBm + 18 dB margin [21])
Transmitter antenna gain	Omni-directional in azimuth 2 dBi in elevation
Receiver antenna gain	25 dBi
Half power beamwidth of receiver horn antenna	10°
Sampling frequency	16 GHz

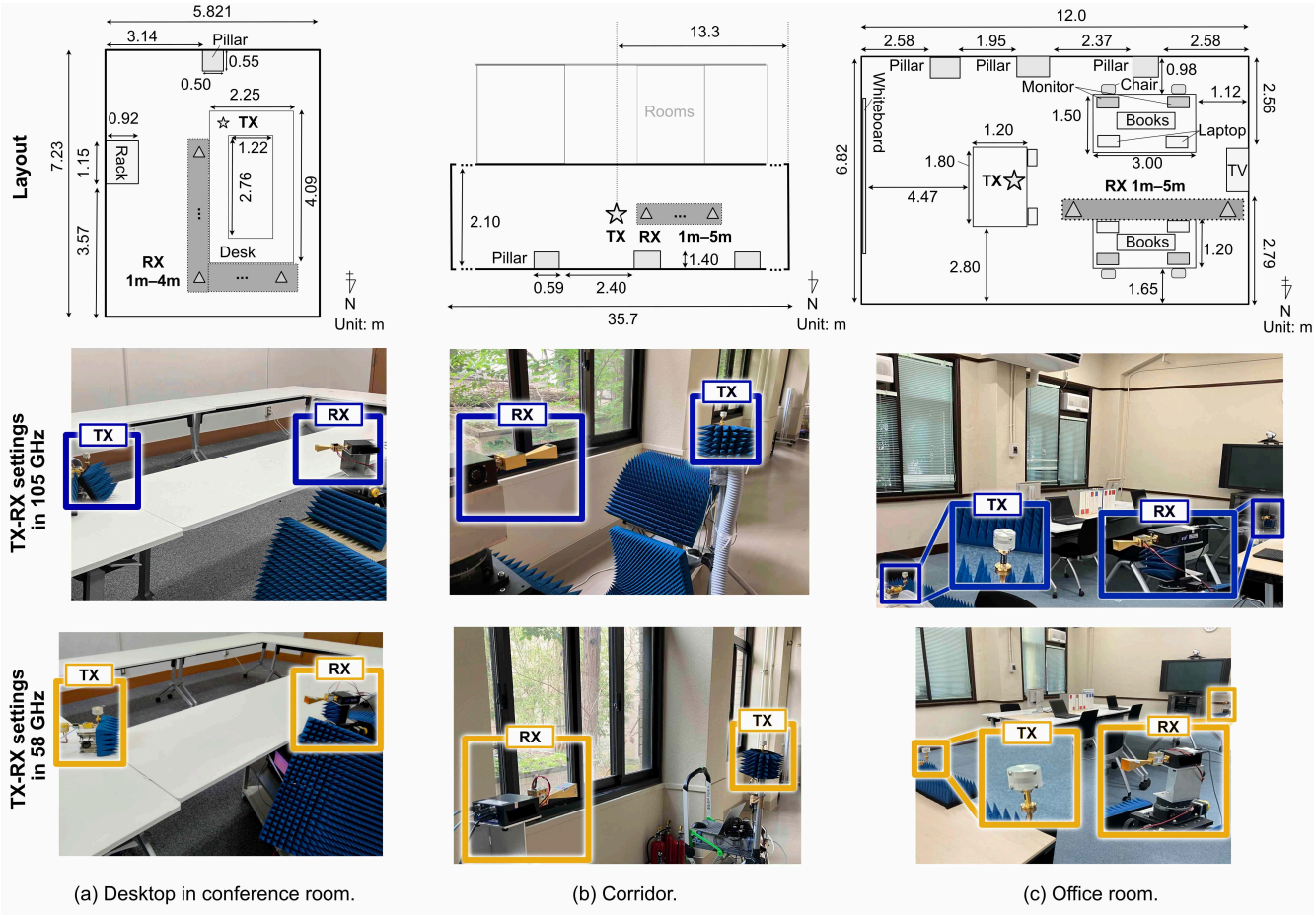

Fig. 2. Measurement environment for 105 GHz and 58 GHz measurement campaigns in indoor short-range scenarios.

60 GHz channel-sounding system. Similarly, we developed a channel-sounding system in the 60 GHz band with a minimal modification to the 105 GHz channel-sounding system as shown in Fig. 1(b). The RX was equipped with a 25 dBi horn antenna and was also rotatable in the azimuth plane. The TX was equipped with an omnidirectional antenna in the azimuth plane. The technique used to obtain the PDPs is the same as the 105 GHz channel-sounding except for the parameter settings. The sounding signal of the pseudo-random sequence was generated with a center frequency of 3 GHz and a bandwidth of 2 GHz, which allows us to obtain the PDP with the time resolution of 0.3125 ns. The sounding signal is up-converted to the radio frequency of 58.32 GHz. The received signal is down-converted to the center frequency of 3 GHz and is sampled by the same oscilloscope. The detailed parameters in this measurement are further shown in Table II.

B. Measurement Scenarios and Environments

Desktop in conference room. This measurement was conducted in a small indoor conference room environment motivated by the use case of exchanging large amounts of data between individuals in a conference room. The room size was 5.8 m × 7.1 m × 3.0 m. The TX was placed on one of the desks, which is aligned in a rectangular shape, at a height of 0.15 m from the desk surface as shown in Fig. 2(a). The RX was placed at the edge of the desk at a distance of 1–4 m from the TX.

Corridor. This measurement was conducted in an indoor corridor environment, which possesses an immoderate aspect ratio compared to the aforementioned indoor rooms. Fig. 2(b) shows the overview and picture of this environment. The entire size of the corridor was 35.7 m × 2.1 m × 3.0 m. Both TX and RX are placed at the height of 1.3 m from the ground level to consider the scenario where device-to-device communication is performed among people holding smartphones while standing in this location.

Office room. This measurement was conducted in an indoor office room environment, which is larger than the small indoor conference room environment. Fig. 2(c) shows the schematic overview and picture of this measurement environment. The room size was 6.8 m × 12.0 m × 3.0 m. Inside this room, we placed office furniture, such as monitors, laptops, and books as shown in Fig. 2(c). Moreover, a whiteboard was attached to the east wall, and the television was placed on the opposite side. The TX was placed near the center of the room, while RX was placed between the two separated office desks at a distance ranging from 1 m to 5 m from the TX.

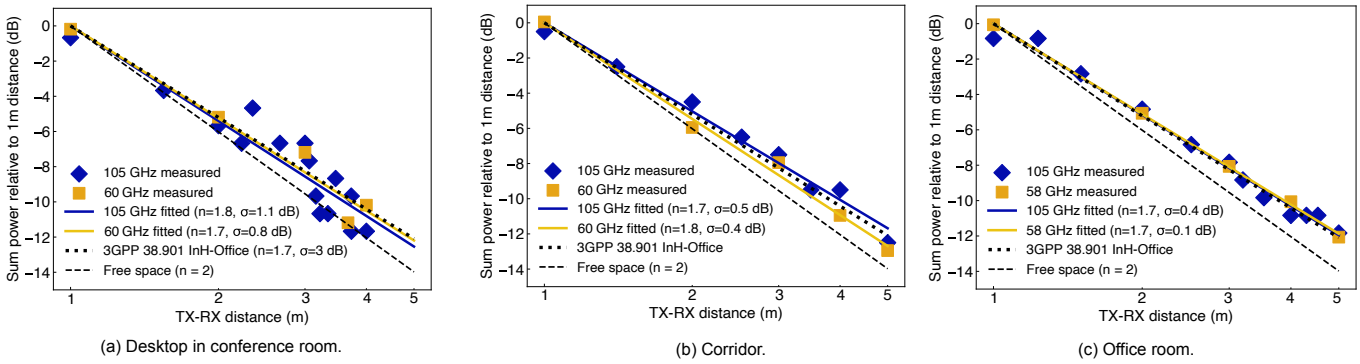

Fig. 3. Path loss models extracted from the measurements in 105 GHz and 60 GHz.

We recorded the PDP while mechanically rotating the RX antenna at the corresponding RX positions. In more detail, we first aligned the RX horn antenna toward the TX omnidirectional antenna and recorded the first PDP. We then rotated the RX horn antenna with the angular step of 5 degrees and recorded the PDP in each RX antenna rotation to cover 360 degrees. This procedure results in 72 PDP records per RX position. Based on the PDPs, we calculated parameters related to the near free space reference distance (CI) path-loss model, which is detailed in the next section. For the sake of notation, we refer to each PDP obtained by the directional antennas as a "directional PDP," while we refer to the set of 72 directional PDPs obtained with all RX antenna rotation angles as an "omnidirectional PDP," because the sum of the 72 PDPs is nearly equivalent to the PDP obtained by employing an omnidirectional RX antenna.

III. Path-Loss Model for 105 GHz Indoor Short-Range Communications

A. Close-in Free-Space Reference Distance Path-Loss Model

As a path-loss model, we adopt the CI path-loss model, which is well-accepted in various path-loss modeling campaigns [9]. Moreover, the standard channel model developed by the 3rd generation partnership project (3GPP) currently adopts this model in the same scenario as the indoor short-range communications as "indoor hotspot office (InH)" in the line-of-sight (LoS) condition [20] for up to the 100 GHz; hence, to naturally bridge this model for above-100 GHz, we first adopt this CI path loss model.

The CI path loss model possesses a mathematically simplified structure, where the path loss at reference distance d_0 is assumed to be the free-space path loss, and the path loss at an arbitrary distance $d \geq d_0$ exponentially increases with d/d_0. The model is formulated as follows [9]:

$$\mathrm{PL}(d,f) = \mathrm{FSPL}(d_0,f) + 10n\log_{10}(d/d_0) + \chi_\sigma,$$

where $\mathrm{PL}(d,f)$ and $\mathrm{FSPL}(d_0,f)$ denote the path loss in the decibel scale at distance d and at center frequency f in giga-hertz and the free-space path loss in the decibel scale at reference distance d_0 and at the same center frequency, respectively. The terms n and $\chi_\sigma \sim \mathcal{N}(0,\sigma^2)$ denote the path loss exponent and the shadow fading term, respectively. $\mathrm{FSPL}(d_0,f)$ is further expressed by $32.4 + 20\log_{10}(d_0) + 20\log_{10}(f)$ dB. In the 3GPP InH LoS model, the reference distance is set to be 1 m. We also set the distance to be 1 m; hence, the problem narrows down to deriving path loss exponent n and standard deviation σ of the shadow fading term from the recorded omnidirectional PDPs for each measurement scenario.

B. Path Loss Parameter Extraction Methodology

We extracted the parameters of the path loss model (i.e., path loss exponent n and standard deviation σ) from the recorded omnidirectional PDP. First, from the omnidirectional PDP in each RX location in each scenario, we extract power samples above threshold P_{th}. This threshold is decided according to the ITU-R recommendation [21] that only power samples 18 dB above the noise floor level should be included for multi-path propagation characterizations. The noise floor level is calculated by averaging the power samples obtained without any receiving signals.

Second, we add all extracted power samples in each RX location and calculate the sum of the effective power samples in the above sense. Let $P_{\mathrm{dB},i}^{sce}$ and d_i^{sce} denote the sum of effective power samples in the decibel domain and the TX-RX distance for each RX location $i \in \{1,2,\ldots,I^{sce}\}$ and for each scenario $sce \in \{desktop, corridor, office\}$, respectively. Subsequently, we perform least-squares fitting with a linear model with data points $\left(\log_{10}(d_i^{sce}), P_{\mathrm{dB},i}^{sce}\right)_i^{I^{sce}}$ to derive the path loss exponent n. Finally, we derive σ by calculating the standard deviation of the residual errors that lie between the fitted line and each data point.

C. Results of Path-Loss Model Extracted from Measurement

Fig. 3 shows data points, fitted lines, and extracted path-loss model parameters in each measurement scenario. Note that Fig. 3 shows the loss relative to the received power at the reference distance of 1 m, which was found by the vias term of the fitted line. This figure provides the following two insights as follows:

Identical path loss exponent with 60 GHz result and with 3GPP LoS InH model. In Fig. 3, the slope of the fitted line is in good agreement with both that in the 3GPP LoS InH model and that in the results of 58 GHz for all examined scenarios. More concretely, the path loss exponents in the 105 GHz ranges

from 1.7–1.8, which coincide with both those in the 3GPP LoS InH model and the model found in 60 GHz with the same RX location. For all models, the smaller path-loss exponent (i.e., 1.7) in both the 3GPP LoS InH model and the model found by this measurement than 2 in the free space path-loss model is attributed to the fact that the omnidirectional antennas receive energy from not only a LoS ray but also multipath components in indoor scenarios.

Considering these facts, the 105 GHz retains the same amount of energy in the multipath components (excluding the difference in FSPL) regardless of the general concern that the THz band suffers from less energy of reflective multipath components with scattering on the surface of the reflective objects [22]. Hence, we can conclude that at least for indoor scenarios, the path loss models developed under 100 GHz can be easily generalized for 105 GHz. In Sec III-D, we further validate this conclusion by showcasing the angular characteristics of the multipath effects in both 105 GHz and 60 GHz results obtained in the identical location.

Larger power dispersion on desk in both 60 GHz and 105 GHz. From Fig. 3, we can find that the scenario of the desktop in a conference room (Fig. 3(a)) leads to more power dispersion to the other scenarios (Figs. 3(b) and 3(c)). This is attributed to the observed power of the LoS ray affected by the ground reflection ray from the desk. More concisely, the LoS ray and the reflective ray from the desk could not be resolved in this measurement setup (even with the 4 GHz bandwidth), resulting in constructive and destructive effects depending on the RX positions. This effect occurs at 60 GHz in our measurement and was also found in the standardization of the IEEE 802.15.3c 60 GHz WPAN [23]. Hence, this effect should be considered in the design of communication systems in this band.

D. Analysis of Multipath Characteristics

Finally, we analyze the multipath characteristics by using all the recorded PDPs at an example RX position in each measurement scenario, where the angular characteristics of the multipath components are extracted and are related to the environmental layouts. As an example, we take the RX positions where the TX-RX distance was 2 m, 3 m, and 2 m for the desktop, corridor, and office scenarios, respectively. At each RX position, we plot the maximum power peak in the recorded PDPs for each RX angle in the form of a polar plot, where the angle of arrival of the multi-path components can be identified with the power. Note that this plot is affected by the antenna patterns for each multipath component, which necessitate the usage of the same receiver antenna patterns for 58 GHz and 105 GHz. Hence, prior to the analysis, we confirmed that the both antenna patterns are identical as shown in Fig. 4.

Fig. 5 shows the measured multipath characteristics for each RX antenna angle in both the 105 GHz and 60 GHz bands. In Fig. 5, we can find similar multipath characteristics in both bands in the sense that several reflective paths arrived while holding similar angles of arrivals and powers, particularly for the desktop and corridor environments. Therein, the difference

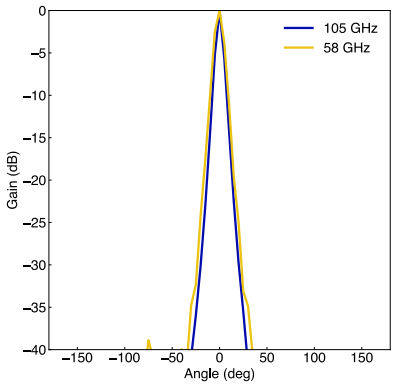

Fig. 4. Antenna pattern of the receiver horn antennas for 58 GHz and 105 GHz.

in the received powers relative to that in the LoS ray between the 105 and 60 GHz bands was within –5 dB at most, and the significant difference in the angle of arrivals between these bands were not identified. Moreover, we can identify that all multipath components that hold strong powers in the 105 GHz band can be explained by the first- or second-order reflection from the walls as in those in the 60 GHz band. These results suggest that an accurate channel simulation in the 105 GHz may be possible with a deterministic ray-tracing simulation as has been done in several standardization efforts for the 60 GHz WLAN systems [24]. Moreover, these results suggest that a beam-switching mechanism designed for the 60 GHz WPAN/WLAN in case of non-LoS conditions [25] may also be feasible in the 105 GHz bands, because the identified multipaths retain similar power levels.

Overall, the signals in the 105 GHz bands retain similar indoor multipath characteristics to those in the 60 GHz band in terms of both path-loss exponent and angular characteristics. Hence, these results suggest the hypothesis that a channel model and various system designs for 60 GHz indoor WPANs/WLANs may be generalized for the 105 GHz bands. The feasibility of this generalization should be further investigated in future works.

IV. Conclusion

This paper has presented the wideband indoor measurement campaign conducted at 105 GHz with a bandwidth of 4 GHz in a conference room desktop, corridor, and office room environments. For this purpose, we developed the channel-sounding system that measures a PDP with RX antenna rotations in the azimuth plane. Moreover, we also developed the 60 GHz channel-sounding system with the bandwidth of 2 GHz band with a slight modification of the 105 GHz channel-sounding system to understand the 105 GHz channel characteristics compared to those in the 60 GHz band. The measurement demonstrated the affinity of the channel characteristics in these two bands in terms of the path loss exponent and angular characteristics. The affinity in the path loss exponent suggests the possibility that indoor path loss models in the 60 GHz band (e.g., the 3GPP InH LoS model in the 38.901 TR developed up to 100 GHz) can be generalized for the 105 GHz. Moreover, the affinity in the power-angular

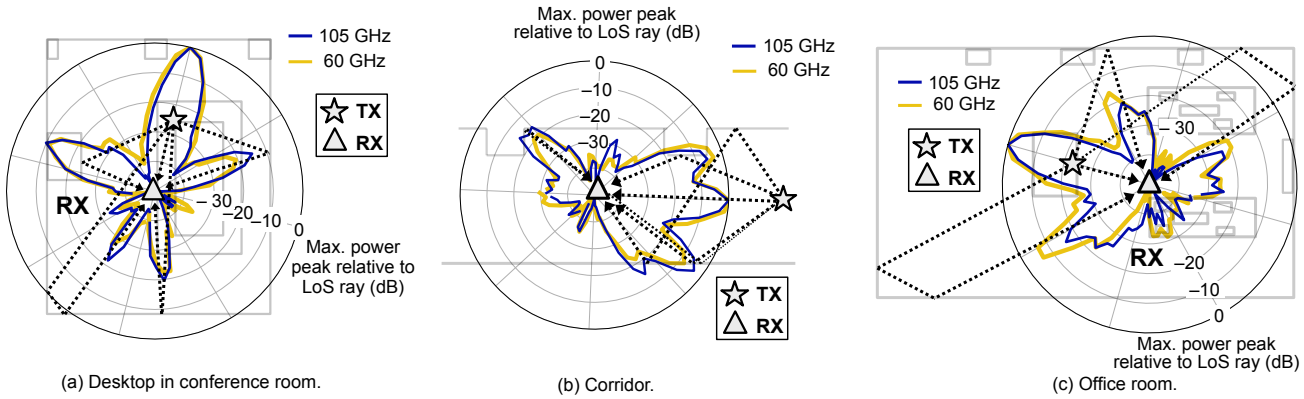

Fig. 5. Example of measured multipath characteristics in 105 GHz and 60 GHz overlayed with environmental layouts.

characteristics in the multipath component suggests the applicability of the 60 GHz beamforming for NLoS cases to the 105 GHz bands, regardless of the general concern that the THz band suffers from reduced powers of the specular reflective paths due to more extensive scattering effects. Our future work includes the investigation of the statistical characteristics of angular and delay spreads in both bands and developing spatiotemporal small-scale channel models applicable to the 100–110 GHz band. Moreover, the multipath characteristics with respect to the anttena rotation in elevation angles should be investiagted.

Acknowlegement

These results were obtained from the commissioned research (No. 04201) by the National Institute of Information and Communications Technology (NICT), Japan.

References

[1] C.-X. Wang *et al.*, "On the road to 6G: Visions, requirements, key technologies, and testbeds," *IEEE Commun. Surv. Tut.*, vol. 25, no. 2, pp. 905–974, Apr. 2023.

[2] S. Kim and A. G. Zajić, "Statistical characterization of 300-GHz propagation on a desktop," *IEEE Trans. Veh. Technol.*, vol. 64, no. 8, pp. 3330–3338, Aug. 2015.

[3] R. Takahashi, K. Shibata, A. Ghosh, and M. Kim, "Validation of 300 GHz channel sounder through indoor multipath measurements," *IEICE Commun. Express*, vol. 12, no. 6, pp. 271–276, Jun. 2023.

[4] H. Sawada *et al.*, "Terahertz propagation modeling for office and corridor environments," *in Proc. EuCAP 2023*, Florence, Italy, Mar. 2023, pp. 1–4.

[5] A. Schultze, F. Undi, M. Peter, W. Keusgen, and T. Eichler, "Angle-resolved THz channel measurements at 300 GHz in a conference room environment," *in Proc. URSI GASS 2021*, Rome, Italy, Aug. 2021, pp. 1–4.

[6] V. Petrov, T. Kurner, and I. Hosako, "IEEE 802.15.3d: First standardization efforts for sub-terahertz band communications toward 6G," *IEEE Commun. Mag.*, vol. 58, no. 11, pp. 28–33, Nov. 2020.

[7] Y. Xing, O. Kanhere, S. Ju, and T. S. Rappaport, "Indoor wireless channel properties at millimeter wave and sub-terahertz frequencies," *in Proc. IEEE GLOBECOM 2019,* Waikoloa, HI, USA, Dec. 2019, pp. 1–6.

[8] Y. Xing and T. S. Rappaport, "Millimeter wave and terahertz urban microcell propagation measurements and models," *IEEE Commun. Lett.*, vol. 25, no. 12, pp. 3755–3759, Dec. 2021.

[9] S. Ju and T. S. Rappaport, "142 GHz multipath propagation measurements and path loss channel modeling in factory buildings," *arXiv* Feb. 2023. [Online]. Available: http://arxiv.org/abs/2302.12142.

[10] L. Pometcu and R. D'Errico, "An indoor channel model for high data-rate communications in D-Band," *IEEE Access*, vol. 8, pp. 9420–9433, Dec. 2019.

[11] S. Le Hong Nguyen, J. Jarvelainen, A. Karttunen, K. Haneda, and J. Putkonen, "Comparing radio propagation channels between 28 and 140 GHz bands in a shopping mall," *arXiv*, Dec. 2017. [Online]. Available: http://arxiv.org/abs/1712.09438

[12] N. A. Abbasi, A. Hariharan, A. M. Nair, and A. F. Molisch, "Channel measurements and path loss modeling for indoor THz communication," *in Proc. EuCAP 2020,* held online, pp. 1–5, Mar. 2020.

[13] D. Dupleich, R. Müller, S. Skoblikov, M. L. G. Del Galdo, and R. Thomä, "Characterization of the propagation channel in conference room scenario at 190 GHz," *in Proc. EuCAP 2020,* held online, pp. 1–5, Mar. 2020.

[14] S. Kim, W. T. Khan, A. Zajić, and J. Papapolymerou, "D-Band channel measurements and characterization for indoor applications," *IEEE Trans. Antennas Propag.*, vol. 63, no. 7, pp. 3198–3207, Jul. 2015.

[15] S. Li *et al.*, "Measurement-based analysis and modeling of channel characteristics in an indoor-office scenario at 100 GHz," *in Proc.* IEEE VTC2023-spring, Florence, Italy, Jun. 2022, pp. 1–7.

[16] "Technical Specification Group Radio Access Network; NR; User Equipment (UE) radio transmission and reception; Part 2: Range 2 Standalone," 3GPP TS 38.101-2 Release 17, Sep. 2022.

[17] S. Kato *et al.*, "Single carrier transmission for multi-gigabit 60-GHz WPAN systems," *IEEE J. Sel. Areas Commun.*, vol. 27, no. 8, pp. 1466–1478, Oct. 2009.

[18] IEEE Computer Society, "IEEE Std 802.11adTM-2012," Apr. 2012

[19] [Online]. Available: https://www.keysight.com/jp/ja/assets/7018-05100/configuration-guides/5992-1326.pdf

[20] "Study on channel model for frequencies from 0.5 to 100 GHz," 3GPP TR 38.901 version 17.0.0 Release 17, Mar. 2022.

[21] "Multipath propagation and parameterization of its characteristics," Recommendation ITU-R P.1407-8, Sep. 2021.

[22] V. Petrov, J. Kokkoniemi, D. Moltchanov, J. Lehtomaki, Y. Koucheryavy, and M. Juntti, "Last meter indoor terahertz wireless access: Performance insights and implementation roadmap," *IEEE Commun. Mag.*, vol. 56, no. 6, pp. 158–165, Jun. 2018.

[23] Y. Shoji, H. Sawada, C.-S. Choi, and H. Ogawa, "A modified SV-model suitable for line-of-sight desktop usage of millimeter-wave WPAN systems," *IEEE Trans. Antennas Propag.*, vol. 57, no. 10, pp. 2940–2948, Oct. 2009.

[24] Y. Koda R. Ouyang N. Ohmi, and H. Harada, "Survey, taxonomy, and unification of standard mmWave channel models for WPAN, WLAN, and cellular systems in 6G," TechRxiv. Preprint. [Online] Available: https://doi.org/10.36227/techrxiv.21522711.v2

[25] Junyi Wang *et al.*, "Beam codebook based beamforming protocol for multi-Gbps millimeter-wave WPAN systems," *IEEE J. Sel. Areas Commun.*, vol. 27, no. 8, pp. 1390–1399, Oct. 2009.